

Viscous oscillatory flow about a circular cylinder at small to moderate Strouhal number

By H. M. BADR†, S. C. R. DENNIS, S. KOCABIYIK‡
AND P. NGUYEN

Department of Applied Mathematics, University of Western Ontario, London,
Ontario N6A 5B7, Canada

(Received 15 December 1994 and in revised form 28 July 1995)

The transient flow field caused by an infinitely long circular cylinder placed in an unbounded viscous fluid oscillating in a direction normal to the cylinder axis, which is at rest, is considered. The flow is assumed to be started suddenly from rest and to remain symmetrical about the direction of motion. The method of solution is based on an accurate procedure for integrating the unsteady Navier–Stokes equations numerically. The numerical method has been carried out for large values of time for both moderate and high Reynolds numbers. The effects of the Reynolds number and of the Strouhal number on the laminar symmetric wake evolution are studied and compared with previous numerical and experimental results. The time variation of the drag coefficients is also presented and compared with an inviscid flow solution for the same problem. The comparison between viscous and inviscid flow results shows a better agreement for higher values of Reynolds and Strouhal numbers. The mean flow for large times is calculated and is found to be in good agreement with previous predictions based on boundary-layer theory.

1. Introduction

In the present paper we shall study the time-dependent, two-dimensional flow over an infinitely long circular cylinder, of radius a , which is placed in an oscillatory flow environment. The cylinder is at rest in a flow whose unidirectional oscillations are represented by $U \cos(\omega t)$. Here t is the time and ω is the frequency of oscillation. The motion is assumed to be governed by the Navier–Stokes equations for an incompressible fluid and the flow is laminar. We shall take fixed axes with origin at the centre of the cylinder, and regard the fluid as oscillating. There are two basic parameters in the problem. One is the Reynolds number, defined as $R = 2aU/\nu$, where ν is the coefficient of kinematic viscosity of the fluid. The second is the Strouhal number α , defined as $\alpha = a\omega/U$, which characterizes the frequency of oscillation. We note that α can be interpreted as the ratio between the radius of the cylinder and the oscillation amplitude.

The influence of the Strouhal number on the flow patterns at low Reynolds numbers has been studied extensively. Schlichting (1932) was the first to calculate the flow field

† Permanent address: Mechanical Engineering Department, King Fahd University of Petroleum and Minerals, Dhahran 31261 Saudi Arabia.

‡ Present address: Department of Applied Mathematics, University of Manitoba, Winnipeg, Manitoba R3T 2N2, Canada.

by means of boundary-layer theory. Wang (1965) calculated the total force on a fixed cylinder in a slightly viscous fluid oscillating with a high Strouhal number α using boundary-layer equations. The cases $R\alpha \gg 1$, $R/\alpha \gg 1$ were discussed theoretically by Riley (1965) and Stuart (1966). Each author employed a different method of solution: Riley developed a series solution analogous to the Blasius series in classical boundary-layer theory and Stuart extended a method due to Fetti (1955). Each method leads, essentially, to the same results following a similar amount of manipulative work. From the usual concepts of boundary-layer theory Stuart showed that, for high Reynolds numbers, in addition to the unsteady boundary layer there exists a second boundary layer in which the steady streaming decays to zero. Wang (1968) obtained analytical solutions for the oscillating cylinder at low Reynolds numbers such that $R\alpha \gg 1$, $R/\alpha \ll 1$ using the method of inner and outer expansions. Stuart (1966) first drew attention to the time-averaged thin jet-like flow that is impelled along the axis of oscillation when $R/\alpha \gg 1$. Subsequently, Davidson & Riley (1972) visualized and made measurements of these jet-like flows. More recently Vasantha & Riley (1988) made a very careful numerical study to trace the origin of jets arising in flow over a circular cylinder in an oscillatory viscous flow environment. Numerical solutions were obtained at both infinite and large but finite Reynolds number when $\alpha = 4$ using both the boundary-layer equations and a viscous–inviscid interactive procedure.

In the present work we study the evolution of the unsteady symmetric wake as a function of time and its structure for large values of time at high values of R when $\alpha \leq \pi$. Low Strouhal numbers are chosen for the study since the flow structure in such cases is characterized by extensive vortex formation, interaction and shedding. In general, as α increases the amplitude of free stream oscillations is reduced and so is the size of the separated region (see for example Badr, Dennis & Kocabiyik 1995). This can be correlated with results to be found in other numerical studies and with available experimental data. Experimental studies of the oscillatory flows related to the present problem have been made by Sarpkaya (1986), Williamson (1985), Obasaju, Bearman & Graham (1988), Tatsuno & Bearman (1990). These studies have attempted to relate the motion of the vortices to the force acting on the cylinder. In addition, the vortex motions are explained in terms of the relevant dimensionless parameters: the Reynolds number R and the Keulegan–Carpenter number KC which is defined by $KC = UT/(2a)$, where T is the period of the oscillation. In sinusoidal flow, $KC = \pi/\alpha$; thus KC is proportional to the flow amplitude. Experimental studies show that KC has a stronger influence on flow patterns at higher R than at lower R .

The most recent numerical studies of this problem have been made by Justesen (1991) and Wang & Dalton (1991). Wang & Dalton made a finite-difference study of the sinusoidally oscillating flow past a fixed circular cylinder using the vorticity and stream function formulation. In their work the Reynolds number ranges from 100 to 3000 and the Keulegan–Carpenter number ranges from 1 to 12. Justesen (1991) presented the results of a numerical study of the two-dimensional oscillating flow around a circular cylinder at small and moderate values of the Reynolds number and in the range $0 < KC < 26$. The initial conditions in his work are those of potential flow theory, i.e. initially the vorticity is zero everywhere. Actually the vorticity is singular initially and in the present paper we give a numerical treatment of this problem which takes account of the initial flow when boundary-layer theory applies, and is also valid at later times, when separation has started and the boundary layer thickens. The present numerical method of solution employs boundary-layer

variables but without making any approximation to the Navier–Stokes equations. It adopts basically the same type of solution structure as that used by Badr & Dennis (1985). The accuracy of the numerical scheme was verified by comparing the results with those obtained from the analytical solution at small times (see for example Badr *et al.* 1995). The equations are integrated at later times using an implicit Crank–Nicolson method of integration. The present numerical method can be used to integrate the equations of motion particularly well for high Reynolds numbers because of the employment of the boundary-layer coordinates. The fully numerical method of solution was carried out for $R = 10^3$ when $\alpha = \pi/4$ and $\pi/2$ and $R = 10^4$ when $\alpha = \pi/2$. The case in which $R = 10^3$, $\alpha = \pi/4$ corresponds to the case for which numerical and experimental results have been described by Justesen (1991). It is important to note that numerical calculations obtained in our work are based on the solution of the full Navier–Stokes equations at both small and large times.

2. Governing equations and method of solution

At time $t = 0$, the viscous incompressible fluid surrounding an infinitely long circular cylinder suddenly starts to oscillate along an axis of symmetry in a viscous incompressible fluid. Unidirectional oscillations of the flow are represented by the velocity $U \cos(\omega t)$, where ω is the frequency of the oscillations and t is the time. In practice, modified polar coordinates (ξ, θ) are used, where $\xi = \log(r/a)$, a is the radius of the cylinder, and the origin is taken at the centre of the cylinder.

The motion is two-dimensional and may be described in terms of the usual two simultaneous equations satisfied by the stream function and the scalar vorticity. Dimensionless functions ψ and ζ are used, related to the dimensional stream function and vorticity ψ^* and ζ^* by the equations $\psi^* = Ua\psi$, $\zeta^* = -U\zeta/a$. The dimensionless radial and transverse components of velocity (u, v) obtained by dividing the corresponding dimensional components by U are then given by

$$u = e^{-\xi} \frac{\partial \psi}{\partial \theta}, \quad v = -e^{-\xi} \frac{\partial \psi}{\partial \xi}, \quad (2.1)$$

and the function ζ is defined by

$$\zeta = e^{-\xi} \left(\frac{\partial u}{\partial \theta} - \frac{\partial v}{\partial \xi} - v \right). \quad (2.2)$$

The equations governing the motion can be expressed as

$$e^{2\xi} \frac{\partial \zeta}{\partial \tau} = \frac{2}{R} \left(\frac{\partial^2 \zeta}{\partial \xi^2} + \frac{\partial^2 \zeta}{\partial \theta^2} \right) - \frac{\partial \psi}{\partial \theta} \frac{\partial \zeta}{\partial \xi} + \frac{\partial \psi}{\partial \xi} \frac{\partial \zeta}{\partial \theta}, \quad (2.3)$$

$$\frac{\partial^2 \psi}{\partial \xi^2} + \frac{\partial^2 \psi}{\partial \theta^2} = e^{2\xi} \zeta. \quad (2.4)$$

Here, $\tau = Ut/a$ and R is the Reynolds number defined by $R = 2Ua/\nu$, where ν is the coefficient of kinematic viscosity.

Equations (2.3) and (2.4) are those considered by Collins & Dennis (1973 *a, b*) in the case of the sudden translation of a circular cylinder without oscillation. In the present case oscillation of the flow enters through the Strouhal number α in the

boundary conditions, which may be stated as

$$\psi = \frac{\partial \psi}{\partial \xi} = 0 \quad \text{when} \quad \xi = 0, \quad (2.5)$$

$$e^{-\xi} \frac{\partial \psi}{\partial \xi} \rightarrow \cos(\alpha\tau) \sin \theta, \quad e^{-\xi} \frac{\partial \psi}{\partial \theta} \rightarrow \cos(\alpha\tau) \cos \theta \quad \text{as} \quad \xi \rightarrow \infty. \quad (2.6)$$

The set of conditions (2.5) and (2.6) must be satisfied for all $\tau > 0$ and for all θ such that $0 \leq \theta \leq \pi$, and moreover, the flow will be assumed to remain symmetrical about the direction of motion. Then both functions ψ and ζ are anti-symmetrical about $\theta = 0$ and $\theta = \pi$ and, in particular,

$$\psi(\xi, \theta) = \zeta(\xi, \theta) = 0 \quad \text{when} \quad \theta = 0, \quad \theta = \pi. \quad (2.7)$$

In the present analysis the calculations are carried out on the basis of the method of solution adopted by Collins & Dennis (1973*a*) in which the functions ψ and ζ were expressed in the form of the series

$$\psi(\xi, \theta, \tau) = \sum_{n=1}^{\infty} f_n(\xi, \tau) \sin n\theta, \quad \zeta(\xi, \theta, \tau) = \sum_{n=1}^{\infty} g_n(\xi, \tau) \sin n\theta \quad (2.8a, b)$$

to determine the initial flow in the boundary-layer mainly by analytical methods for small values of τ . The equations governing the functions in (2.8*a,b*) can be obtained by substitution in (2.3) and (2.4). They have been given by Collins & Dennis (1973*b*) and their solution is required in the present case subject to the conditions

$$f_n = \frac{\partial f_n}{\partial \xi} = 0 \quad \text{when} \quad \xi = 0, \quad (2.9)$$

for all n . As a consequence of the condition (2.6) we must also have that, for all n ,

$$g_n(\xi, \tau) \rightarrow 0 \quad \text{as} \quad \xi \rightarrow \infty. \quad (2.10)$$

Finally, the condition (2.6) implies that

$$e^{-\xi} \frac{\partial f_n}{\partial \xi} \rightarrow \cos(\alpha\tau) \delta_{n,1}, \quad e^{-\xi} \frac{\partial f_n}{\partial \theta} \rightarrow \cos(\alpha\tau) \delta_{n,1} \quad \text{as} \quad \xi \rightarrow \infty, \quad (2.11)$$

where $\delta_{m,n}$ is the Kronecker delta symbol defined by

$$\delta_{m,n} = 1 \quad \text{if} \quad m = n, \quad \delta_{m,n} = 0 \quad \text{if} \quad m \neq n.$$

It may now be shown, following Collins & Dennis (1973*a*), that (2.9) and (2.11) can be combined to give further sets of conditions of global type, namely

$$\int_0^{\infty} e^{(2-n)\xi} g_n(\xi, \tau) d\xi = 2 \cos(\alpha\tau) \delta_{n,1}, \quad (2.12)$$

where $\delta_{n,1}$ has the significance in (2.11).

In the initial stages of the motion the boundary-layer coordinate x can be introduced by the transformation

$$\xi = kx, \quad k = 2(2\tau/R)^{1/2}. \quad (2.13)$$

This is employed to transform all the appropriate equations together with the scaling

of variables

$$f_n = kF_n, \quad g_n = \frac{G_n}{k}. \quad (2.14)$$

The differential equations and the boundary conditions to be satisfied by the functions F_n and G_n are given by Collins & Dennis (1973*a,b*).

3. Numerical integration procedure

The expansions in powers of τ obtained by Badr *et al.* (1995) enable properties of the flow to be calculated for large R and small τ , although nothing precise can be said about the region of convergence of the series. In order to calculate the flow for any Reynolds number and large enough time, the numerical method of integration given by Badr & Dennis (1985) may be used. An implicit method of integration of Crank–Nicolson type is used, and a given approximation is obtained by truncating the series (2.8*a, b*). This is done by setting to zero all functions $F_n(x, \tau)$ and $G_n(x, \tau)$ for $n > n_0$, where n_0 is an integer defining the order of truncation.

The essential details of the procedure have been given by Badr & Dennis (1985). Only a few functions $F_n(x, \tau)$ and $G_n(x, \tau)$ are needed to describe the motion for small τ in view of the initial structure given by Badr *et al.* (1995, equation (3.7)). More functions are added as integration proceeds and the parameter n_0 actually refers to the maximum number of terms used in each of the series (2.8*a,b*) during the integration. The value $n_0 = 40$ was found to be more than adequate over the quite large time range of calculations. An illustration of the effect of varying the number of terms used in the series (2.8*a,b*) will be given when the results are described in the next sections. It is also necessary to use a small time step for small τ . The reason is that the expansions of $F_n(x, \tau)$ and $G_n(x, \tau)$ involve odd powers of k and hence all derivatives with respect to τ after some stage are singular at $\tau = 0$. The problem does not arise in the boundary-layer case, where $k = 0$. For the cases of finite R considered the integrations were all started by taking 10 time steps $\Delta\tau = 10^{-4}$. The time step was then increased to $\Delta\tau = 10^{-3}$ for the next 10 steps and then to $\Delta\tau = 10^{-2}$ for the next 10. Finally $\Delta\tau = 0.025$ was taken for the rest of the solution. The grid size in the x -direction was taken as $\Delta x = 0.05$. The values of grid sizes were to some extent chosen to be comparable with those used by Badr & Dennis (1985), since these were found to be satisfactory and were checked carefully. A few comparable checks on different grids were made at one or two values of τ during the present calculations. Moreover, the solutions obtained by fully numerical means are compared with the results obtained using expansions in powers of τ ; these comparisons indicate that the solutions are quite accurate. Finally, we may note that the numerical method described may be used to continue the solution for increasing τ in terms of the physical coordinate ξ when the boundary layer thickens. The same methods may be used to integrate (2.10) and (2.11) subject to the boundary conditions in terms of these coordinates. However in the present paper only cases for which $R \geq 1000$ are presented and it is possible to work in terms of the boundary-layer coordinate x over the entire range of τ considered. The maximum value of x was $x_M = 8$.

4. Results

The variation of drag coefficients with time is calculated both from the viscous flow and inviscid flow solutions. It may be noted that the present analysis uses the analytical expressions for the surface pressure and drag coefficient obtained by Badr

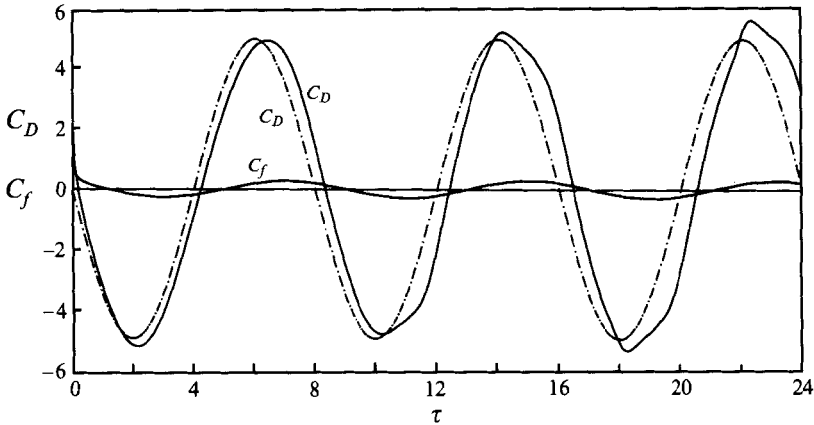


FIGURE 1. Comparison of the variation of C_D with τ at $R = 10^3, \alpha = \pi/4$: —, numerical; - · - · -, potential flow solution.

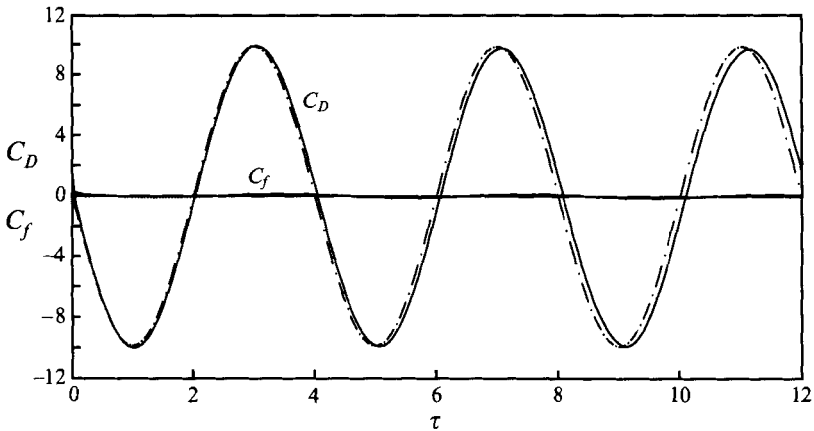


FIGURE 2. Comparison of the variation of C_D with τ at $R = 10^4, \alpha = \pi/2$: —, numerical; - · - · -, potential flow solution.

(1994), who considered oscillating inviscid flow over elliptic cylinders. In his work analytical expressions are given for the drag coefficient, the lift coefficient, and their variation with time. Similar analytical expressions are also given in Badr's work for the special cases of circular cylinders and inclined flat plates in oscillating inviscid flows.

A dimensionless drag coefficient C_D is defined by $C_D = D/\rho U^2 a$ where D is the total drag on the cylinder. The viscous drag coefficient can be obtained from

$$C_D = \frac{4}{R} \int_0^\pi \left(\zeta - \frac{\partial \zeta}{\partial \xi} \right)_{\xi=0} \sin \theta d\theta, \tag{4.1}$$

in which the first term in the integral gives the friction drag coefficient C_f and the second the pressure drag coefficient C_p , where $C_D = C_f + C_p$. The inviscid flow properties can be obtained by solving the unsteady Euler equation for the special case under consideration in which the free stream velocity changes according to $U \cos \omega t$.

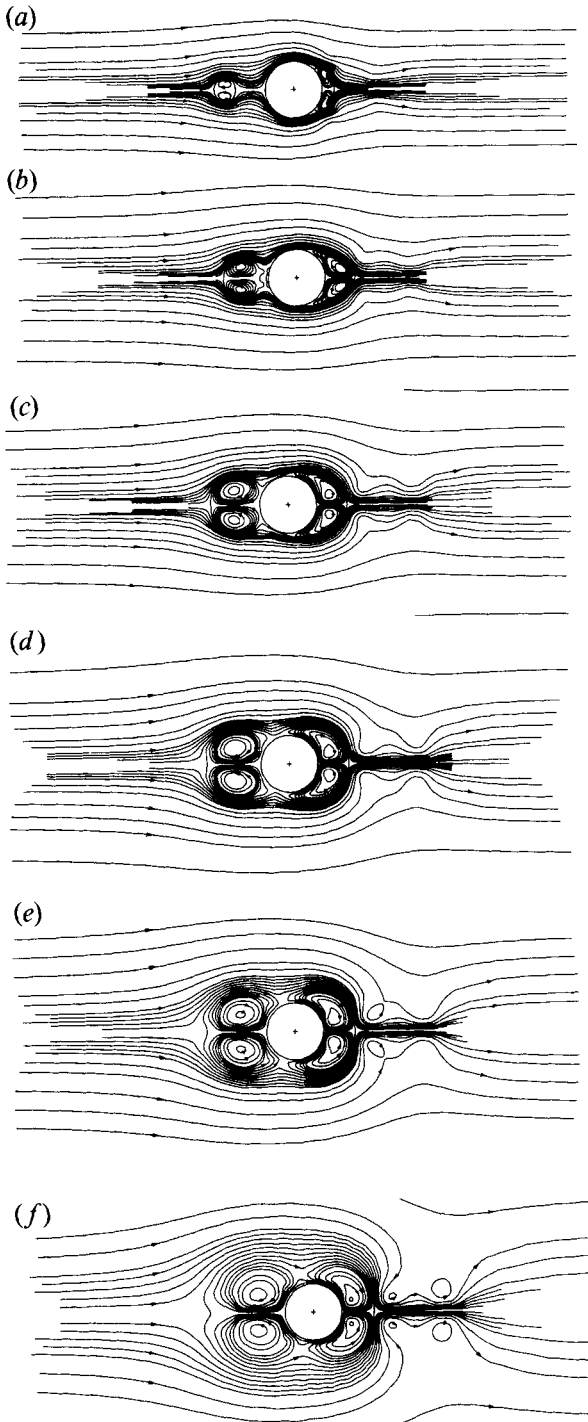


FIGURE 3 (a-f). For caption see page 225.

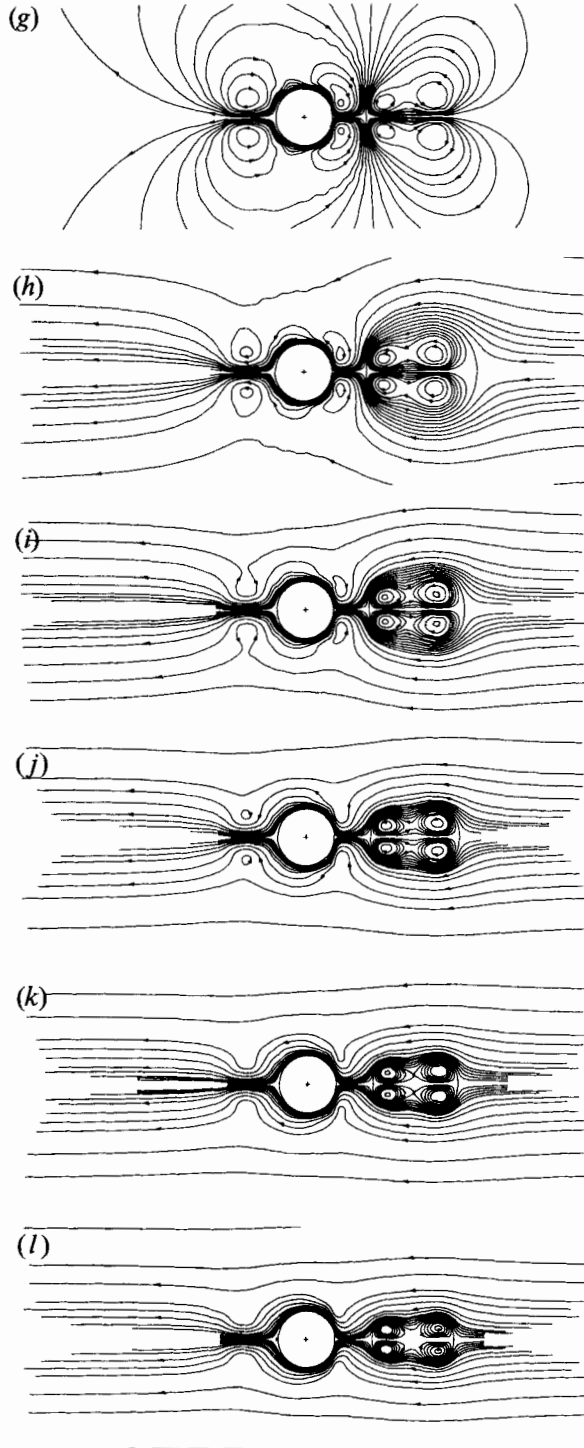


FIGURE 3 (g-l). For caption see page 225.

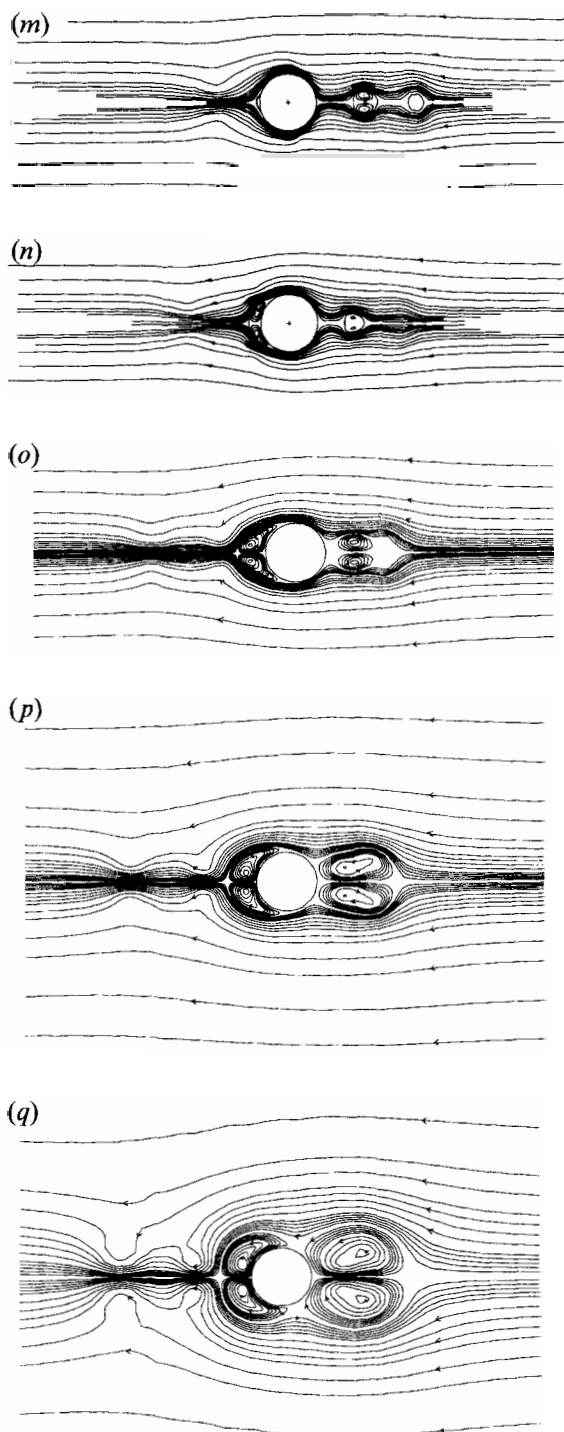


FIGURE 3 (*m-q*). For caption see page 225.

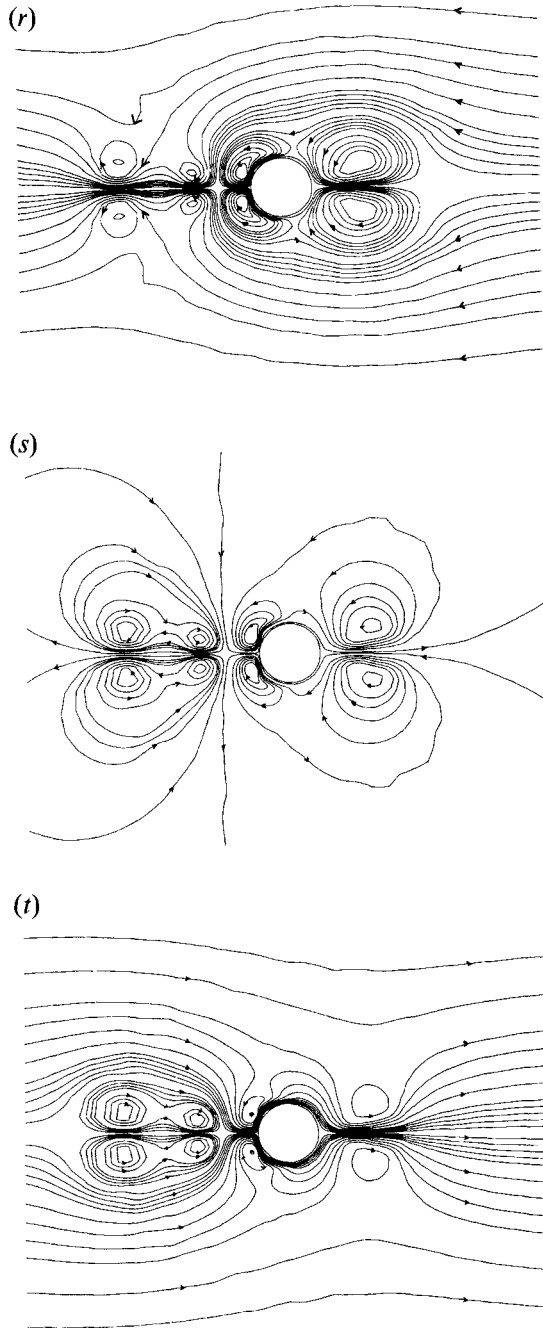


FIGURE 3 (*r-t*). For caption see page 225.

The drag coefficient is deduced from the analysis of Badr (1994) to be

$$C_D = -\pi\alpha \sin \alpha t \quad (4.2)$$

for the potential flow. The calculated values of C_f and C_D based on the expressions (4.1) and (4.2) are plotted in figures 1 and 2 for comparison. These figures show

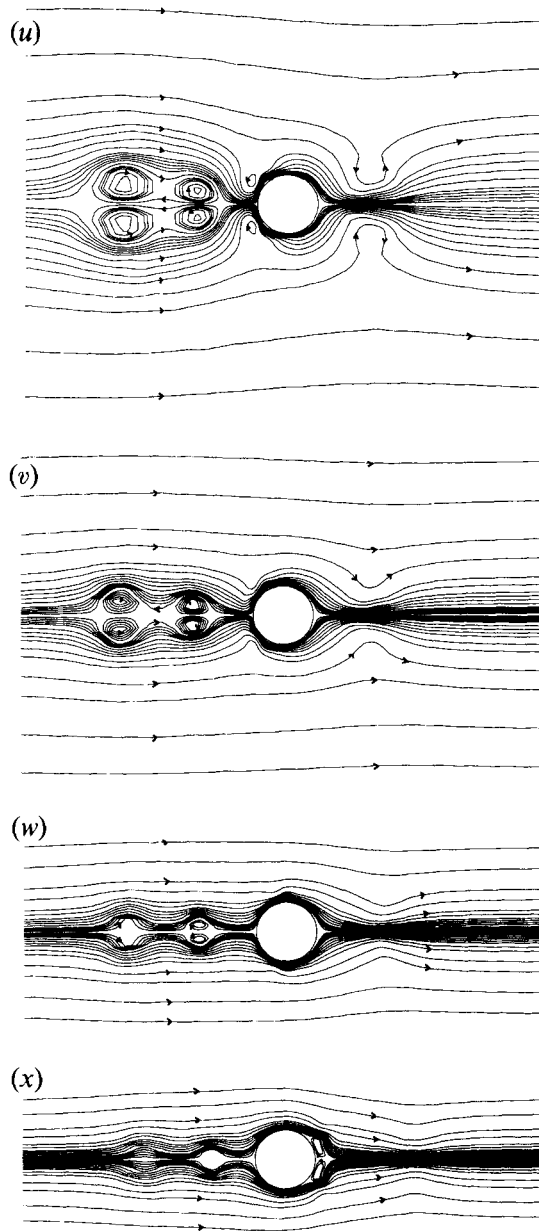


FIGURE 3. Instantaneous streamlines of the flow for $R = 10^3$, $\alpha = \pi/4$ at various times: (a) $\tau = 16.0$, (b) 17.0, (c) 17.5, (d) 17.7, (e) 17.8, (f) 17.9, (g) 18.0, (h) 18.1, (i) 18.2, (j) 18.3, (k) 18.4, (l) 18.5, (m) 19.0, (n) 20.0, (o) 21.0, (p) 21.5, (q) 21.8, (r) 21.9, (s) 22.0, (t) 22.1, (u) 22.2, (v) 22.5, (w) 23.0, (x) 24.0.

that the contribution of frictional forces to the total drag coefficient C_D is relatively small. They also show that the phase difference between the viscous and inviscid flow solutions is small at the start of the motion and increases with the increase of time. The reason for this is that the flow field away from the cylinder is vortex-free at small times. As time increases, vortices are shed away from the cylinder causing changes in the flow field structure. Such changes will cause the flow away from the cylinder

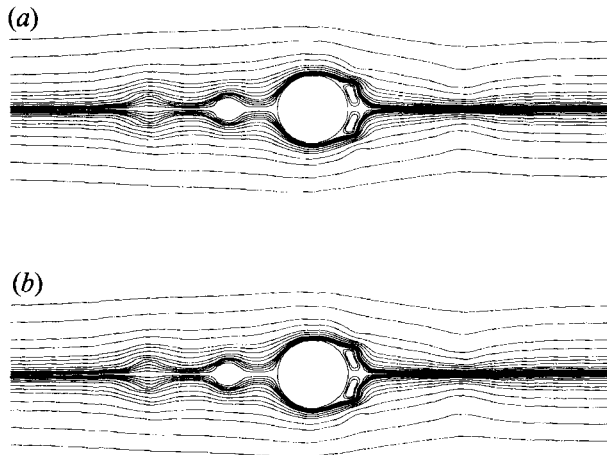


FIGURE 4. Effect of the number of terms n_0 taken in the series (2.8a,b) on the flow patterns at $\tau = 24.0$ for $R = 10^3$, $\alpha = \pi/4$: (a) $n_0 = 15$, (b) $n_0 = 25$.

to deviate from the potential flow. Accordingly, one can assume that there are two dominating flow fields affecting the boundary-layer region. The first is the potential flow field while the second (superimposed on the first) is that resulting from vortical motion. In the present problem the second field has negligible effect at the start of fluid motion but has increasing influence as time increases. Such a field continues to evolve with time until asymptotically approaching a periodic behaviour at large time. Figure 2 shows a small difference between the values of C_D obtained from viscous and inviscid flow solutions. This is expected since the flow oscillations in this case exhibit high frequency and a relatively low amplitude. The effect of both factors is simply an increase of the inertia effect and a decrease in the size of the separated flow region. Both effects will create a pressure field closer to that of potential flow.

The instantaneous streamline patterns are only plotted for the two cases of $R = 10^3$, $\alpha = \pi/4$ and $R = 10^4$, $\alpha = \pi/2$. Figure 3 shows the time variation of the streamline pattern for the first case when τ varies from 16.0 to 24.0. This gives the details of the flow field structure during the third oscillation after the start of the motion. Figure 3(a) shows the streamlines when the free stream is moving to the right at maximum velocity. The values of ψ on the streamlines between the cylinder and the detached vortex starting from the top of the diagram are $\psi = 2.0, 1.5, 1.0, 0.75, 0.5, 0.4, 0.3, 0.2, 0.15, 0.1, 0.08, 0.06, 0.04, 0.02, 0.0, -0.02, -0.04, -0.06, -0.08, -0.1, -0.15, -0.2, -0.3, -0.4, -0.5, -0.75, -1.0, -1.5, -2.0$. In the subsequent diagrams the spacing of streamlines is very similar. The figure shows two pairs of vortices: one is growing in the cylinder wake and the other pair is decaying upstream of the cylinder. One can see the growth of the vortex pair in the cylinder wake and the movement of the other pair towards the cylinder in figures 3(b)–3(d). Figures 3(e) and 3(f), at $\tau = 17.80$ and $\tau = 17.90$ respectively, show the streamline pattern before the free stream comes to complete rest. The same figures also show the formation of another pair of very weak vortices resulting mainly from the high fluid deceleration. Figure 3(g) shows the streamlines when the free stream velocity is zero. The large distances between streamlines far away from the cylinder reflect the very small velocity there while the fluid motion near the cylinder is dominated by vortical motion. Figures 3(h)–(m) show the high rate of decay of the vortices resulting from viscous effects. Figure 3(n) shows the situation when the free stream is moving to the left at maximum

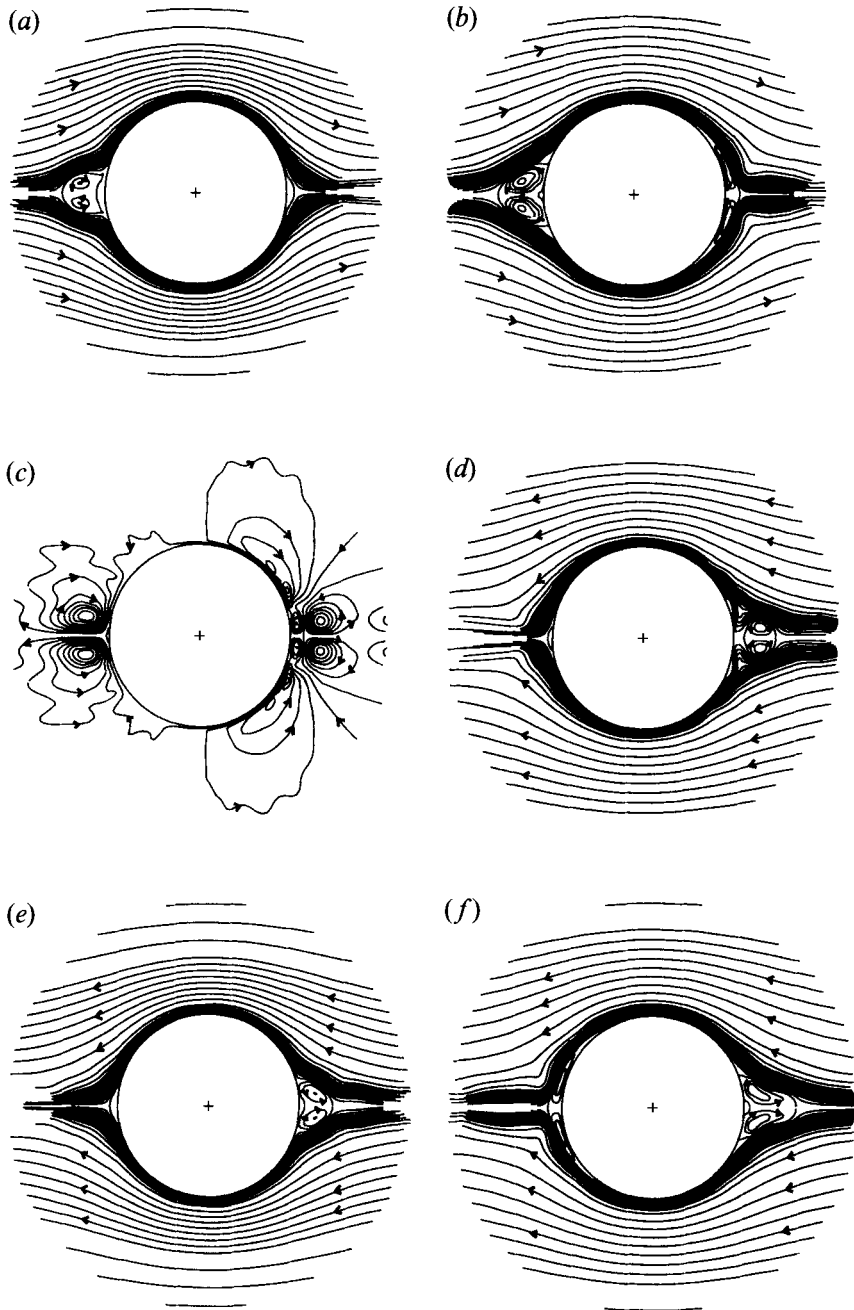


FIGURE 5 (a-f). For caption see next page.

velocity. The figure is very similar to figure 3(a) (only turned through an angle of 180° since the free stream has completed one half-cycle of oscillation). Figures 3(o-r) give additional details of the flow structure as the free stream decelerates before reversing direction at $\tau = 22.0$. Figure 3(s), which shows the streamline pattern when the free stream velocity is zero, is very similar to figure 3(g) when turned through

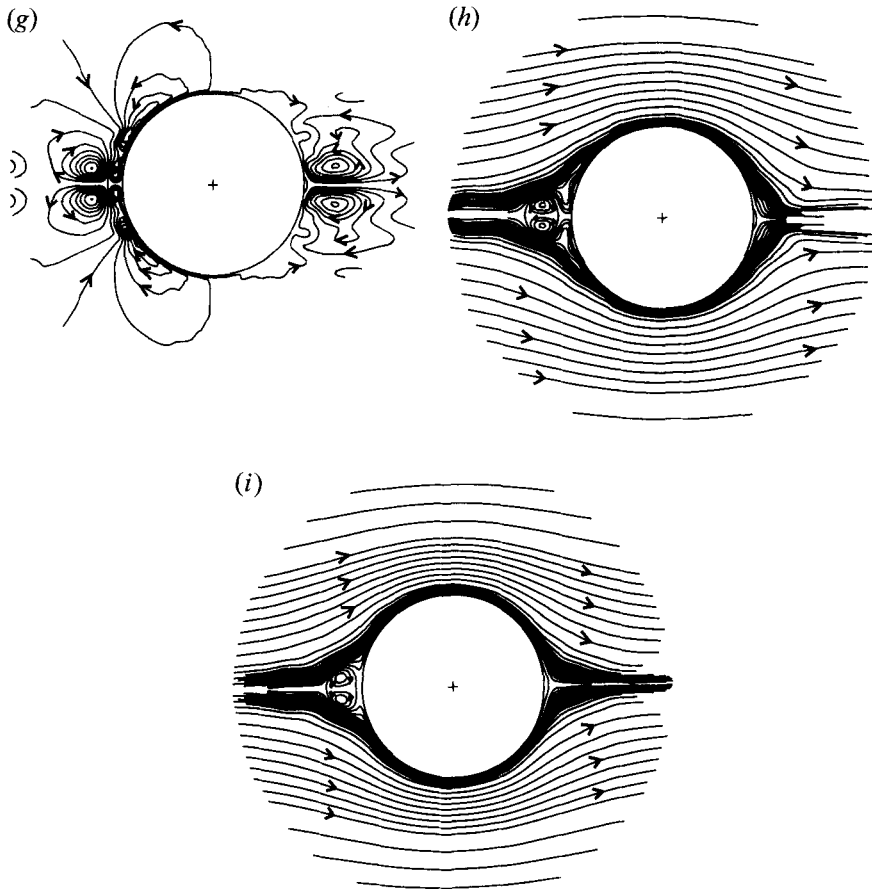


FIGURE 5. Instantaneous streamlines of the flow for $R = 10^4$, $\alpha = \pi/2$ at various times: (a) $\tau = 8$, (b) 8.5, (c) 9.0, (d) 9.5, (e) 10.0, (f) 10.5, (g) 11.0, (h) 11.5, (i) 12.0.

an angle of 180° . Finally, figure 3(x), which shows the flow field at the end of the third complete oscillation ($\tau = 24.0$), similar to the situation at the beginning of that oscillation ($\tau = 16.0$) shown in figure 3(a). The minor differences between figures 3(a) and 3(x) reflect the continuous development of the flow field away from the cylinder because of the vortex shedding and interaction. This flow field has not yet become periodic and requires a larger number of oscillations before reaching exact variations (quasi-state).

In view of the fairly complicated nature of the flow structure, some tests of the adequacy of the number of terms taken in the series (2.8a,b) seems desirable. Some checks were therefore made on the solution for $R = 10^3$, $\alpha = \pi/4$ at the maximum time $\tau = 24$ by increasing the number of terms from 15 to 25. The results for the flow pattern at this time are compared in figures 4(a) and 4(b) for the cases of $n_0 = 15, 25$. The details are seen to be quite comparable at the maximum solution time and they also compare well with figure 3(x).

The time variation of the streamline pattern for the case of $R = 10^4$, $\alpha = \pi/2$ is shown in figure 5(a-i) for selected values of τ between $\tau = 8.0$ and $\tau = 12.0$. The chosen interval represents the third complete oscillation following the start of fluid motion. Figures 5(a), 5(e) and 5(i) represent the situation at the beginning, middle and

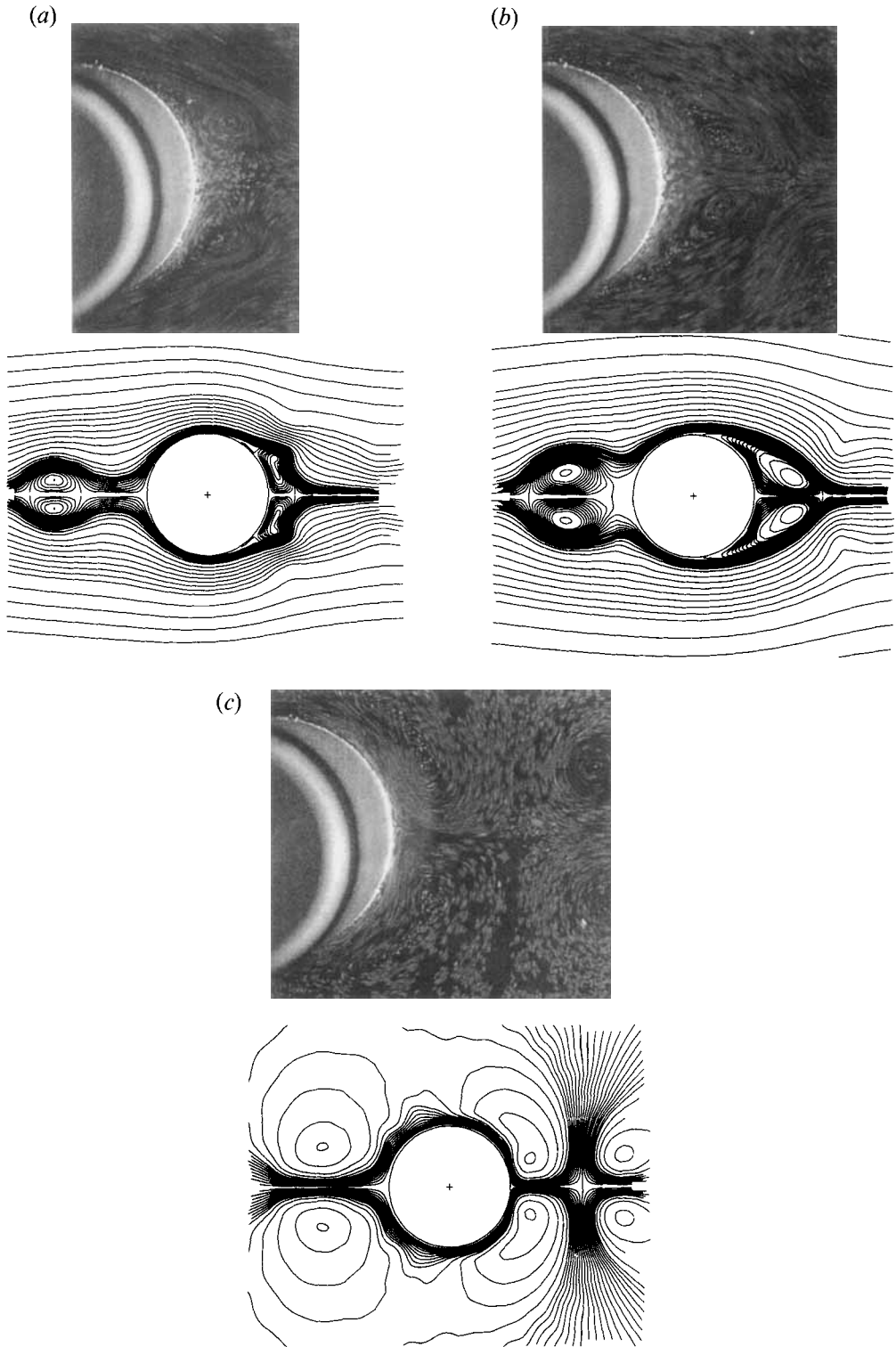


FIGURE 6. Comparison with Justesen's flow visualizations for $R = 10^3$, $\alpha = \pi/4$ and (a) $\tau = 16.0$, (b) $\tau = 17.0$, (c) $\tau = 18.0$.

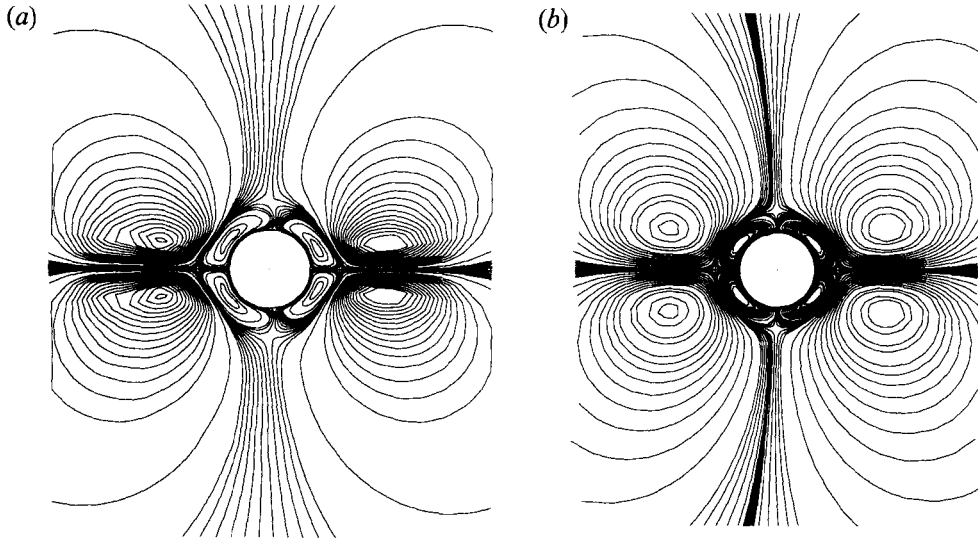


FIGURE 7. Time-averaged flow field over one period of oscillation for (a) $R = 10^3$, $\alpha = \pi/4$ at $\tau = 22.0$ and (b) $R = 10^3$, $\alpha = \pi/2$ at $\tau = 81$.

end of the oscillation, respectively. The velocity of the free stream is maximum in each of these figures. On the other hand, figures 5(c) and 5(g) represent the times at which the free stream velocity is zero. Streamline patterns in figure 5 show that vortices are formed in relatively small areas, leaving the rest of the flow vortex-free. The repetitive nature of the flow field can be observed from the mirror image resemblances between the diagrams for $\tau = 8.00$ and $\tau = 10.00$; $\tau = 8.50$ and $\tau = 10.50$; $\tau = 9.00$ and $\tau = 11.00$; and $\tau = 9.50$ and $\tau = 11.50$. These are given in figures 5(a, e); 5(b, f); 5(c, g) and 5(d, h). This case is like the potential flow case because vortex shedding is restricted to a very small region. Figures 5(a) and 5(i) are almost the same, showing the periodic variation of the flow field at $\tau = 8.00$ and $\tau = 12.00$, respectively.

Figure 6 shows a comparison between the streamline patterns obtained in the present study for the case of $R = 10^3$, $\alpha = \pi/4$ and those obtained experimentally by Justesen (1991). Small deviations between the streamline patterns and experimental work are due to the fact that we did not advance the numerical solution far enough in time to achieve a periodic flow field. To check this the calculated time-averaged flow field over one period of oscillation is plotted in the case of $R = 10^3$, $\alpha = \pi/4$ at $\tau = 22.00$ in figure 7(a). Figure 7(b) shows the mean flow in the case $R = 10^3$, $\alpha = \pi/2$ at $\tau = 81.00$ which is almost steady-state. The streamlines in this figure may be compared with the steady-state streamlines of the mean flow according to the experiments of Masakazu Tatsuno which are shown by Van Dyke (1982) and reproduced here in figure 8. Bearing in mind that the Reynolds number for the flow shown by Van Dyke is considerably lower than that of the present case, it may be noted that, even so, there is very good qualitative agreement between the two diagrams in the boundary-layer region close to the cylinder and that the double boundary-layer structure noted by Riley (1965) and Stuart (1966) in these oscillating flows is very amply confirmed.

The support of the Natural Sciences and Engineering Research Council of Canada for this investigation is gratefully acknowledged. We also acknowledge the interest and support of the King Fahd University of Petroleum and Minerals, Dhahran.



FIGURE 8. Steady-state streamlines of the mean flow according to the experiments of Masakazu Tatsuno (see Van Dyke 1982, p. 23, figure 31).

REFERENCES

- BADR, H. M. 1994 Oscillating inviscid flow over elliptic cylinders with flat plates and circular cylinders as special cases. *Ocean Engng* **21**, 105–113.
- BADR, H. M. & DENNIS, S. C. R. 1985 Time-dependent viscous flow past an impulsively started rotating and translating circular cylinder. *J. Fluid Mech.* **158**, 447–488.
- BADR, H. M., DENNIS, S. C. R. & KOCABIYIK, S. 1995 Initial oscillatory flow past a circular cylinder. *J. Engng Maths* **29**, 255–269.
- COLLINS, W. M. & DENNIS S. C. R. 1973a The initial flow past an impulsively started circular cylinder. *Q. J. Mech. Appl. Maths* **26**, 53–75.
- COLLINS, W. M. & DENNIS S. C. R. 1973b Flow past an impulsively started circular cylinder. *J. Fluid Mech.* **60**, 105–127.

- DAVIDSON, B. J. & RILEY, N. 1972 Jets induced by oscillatory motion. *J. Fluid Mech.* **53**, 287–303.
- FETTIS, H. E. 1955 On the integration of a class of differential equations occurring in the boundary-layer and other hydrodynamic problems. *Proc. 4th Midwestern Conf. on Fluid Mech., Purdue University*, pp. 93–114.
- JUSTESEN, P. 1991 A numerical study of oscillating flow around a circular cylinder. *J. Fluid Mech.* **222**, 157–196.
- OBASAJU, E. D., BEARMAN, P. W. & GRAHAM, J. M. R. 1988 A study of forces, circulation and vortex patterns around a circular cylinder in oscillating flow. *J. Fluid Mech.* **196**, 467–494.
- RILEY, N. 1965 Oscillating viscous flows. *Mathematika* **12**, 161–175.
- SARPKAYA, T. 1986 Force on a circular cylinder in viscous oscillatory flow at low Keulegan–Carpenter numbers. *J. Fluid. Mech.* **165**, 61–71.
- SCHLICHTING, H. 1932 Berechnung ebener periodischer Grenzschichtströmungen *Phys. Z.* **33**, 327–335.
- STUART, J. T. 1966 Double boundary-layers in oscillatory viscous flows. *J. Fluid Mech.* **24**, 673–687.
- TATSUNO, M. & BEARMAN, P. W. 1990 A visual study of the flow around an oscillating circular cylinder at low Keulegan–Carpenter numbers and low Stokes numbers. *J. Fluid Mech.* **211**, 157–182.
- VAN DYKE, M. 1982 *An Album of Fluid Motion*, fig. 31, pp. 23. Stanford: The Parabolic Press.
- VASANTHA, R. & RILEY, N. 1988 On the initiation of jets in oscillatory viscous flows. *Proc. R. Soc. Lond. A* **419**, 363–378.
- WANG, C.-Y. 1965 The resistance on a circular cylinder in an oscillating stream. *Q. Appl. Maths* **23**, 305–312.
- WANG, C.-Y. 1968 On high-frequency oscillatory viscous flows. *J. Fluid Mech.* **312**, 55–68.
- WANG, X. & DALTON, C. 1991 Oscillating flow past a rigid circular cylinder: A finite difference calculation. *Trans. ASME I: J. Fluids Engng* **113**, 377–383.
- WILLIAMSON, C. H. K. 1985 Sinusoidal flow relative to circular cylinders. *J. Fluid Mech.* **155**, 141–174.